1-1-2012

Enhanced hydrogen storage properties of NaAlH4 co-catalysed with niobium fluoride and single-walled carbon nanotubes

Jianfeng Mao
University of Wollongong, jm975@uowmail.edu.au

Zaiping Guo
University of Wollongong, zguo@uow.edu.au

Hua-Kun Liu
University of Wollongong, hua@uow.edu.au

Enhanced hydrogen storage properties of NaAlH4 co-catalysed with niobium fluoride and single-walled carbon nanotubes

Abstract

The effects of single-walled carbon nanotubes (SWCNTs) as a co-catalyst with NbF_5 on the dehydrogenation and hydrogenation kinetics of $NaAlH_4$ were investigated by X-ray diffraction, Fourier transform infrared spectroscopy, differential thermal analysis, temperature-programmed desorption, and isothermal hydrogen ab/desorption techniques. It has been revealed that there is a synergistic effect of SWCNTs and NbF_5 on the de/rehydrogenation of NaAlH4, which improves the hydrogen de/absorption performance when compared to adding either SWCNTs or NbF_5 alone. For example, the apparent activation energy for the first-step and the second-step dehydrogenation of the co-doped NaAlH4 sample is estimated to be 85.9 and 96.2 kJ mol^{-1}, respectively, using Kissinger's approach, which is lower than the pristine, SWCNT-, and NbF_5 doped $NaAlH_4$, respectively, indicating a reduced kinetic barrier. These results are attributed to the active Nb-containing species and the function of F anions, as well as the nanosized pores and high specific surface area of the SWCNTs, which facilitates the dissociation and recombination of hydrogen molecules on its surface and the atomic hydrogen diffusion along the grain boundaries and inside the grains, and decreases the segregation of bulk Al after the desorption. Hence, the combined catalytic mechanism is presented.

Keywords

niobium, fluoride, single, walled, carbon, nanotubes, properties, catalysed, co, naalh4, enhanced, hydrogen, storage

Disciplines

Engineering | Physical Sciences and Mathematics

Publication Details

Mao, J, Guo, Z & Liu, H (2012), Enhanced hydrogen storage properties of NaAlH4 co-catalysed with niobium fluoride and single-walled carbon nanotubes, RSC Advances, 2(4), pp. 1569-1576.

View Article Online / Journal Homepage / Table of Contents for this issue
Dynamic Article Links

RSC Advances

Cite this: *RSC Advances*, 2012, **2**, 1569–1576

www.rsc.org/advances

PAPER

Enhanced hydrogen storage properties of $NaAlH_4$ co-catalysed with niobium fluoride and single-walled carbon nanotubes†

Jianfeng Mao,*[a] Zaiping Guo*[ab] and Huakun Liu[a]

Received 29th August 2011, Accepted 16th November 2011
DOI: 10.1039/c1ra00645b

The effects of single-walled carbon nanotubes (SWCNTs) as a co-catalyst with NbF_5 on the dehydrogenation and hydrogenation kinetics of $NaAlH_4$ were investigated by X-ray diffraction, Fourier transform infrared spectroscopy, differential thermal analysis, temperature-programmed desorption, and isothermal hydrogen ab/desorption techniques. It has been revealed that there is a synergistic effect of SWCNTs and NbF_5 on the de/rehydrogenation of $NaAlH_4$, which improves the hydrogen de/absorption performance when compared to adding either SWCNTs or NbF_5 alone. For example, the apparent activation energy for the first-step and the second-step dehydrogenation of the co-doped $NaAlH_4$ sample is estimated to be 85.9 and 96.2 kJ mol^{-1}, respectively, using Kissinger's approach, which is lower than the pristine, SWCNT-, and NbF_5 doped $NaAlH_4$, respectively, indicating a reduced kinetic barrier. These results are attributed to the active Nb-containing species and the function of F anions, as well as the nanosized pores and high specific surface area of the SWCNTs, which facilitates the dissociation and recombination of hydrogen molecules on its surface and the atomic hydrogen diffusion along the grain boundaries and inside the grains, and decreases the segregation of bulk Al after the desorption. Hence, the combined catalytic mechanism is presented.

Introduction

Clean energy sources such as wind, solar, and hydropower are needed to meet the challenges of global warming and to address the finite nature of fossil fuel based energy resources. However, for the environmentally friendly use of the energy produced by these sources in final applications, a clean, efficient, and safe energy carrier is necessary. Since the development of the proton exchange membrane (PEM) fuel cell, which is fuelled by hydrogen and oxygen, and produces only water, hydrogen has been seen to be the most promising solution.[1] However, the use of hydrogen for fuel-cell powered mobile applications requires materials that not only store hydrogen at high density, but that can operate reversibly at ambient pressure and temperatures below approximately 100 °C.[2]

Among the many materials studied for hydrogen storage, complex hydrides of light metals containing borohydride,[3] amide,[4] and alanate[5,6] anions have high hydrogen capacity and, thus, have been studied extensively. However, the thermodynamic and kinetic properties of the borohydrides limit their ability to cycle hydrogen at low temperatures. On the other hand, the elimination of ammonia gas in using amides for hydrogen storage is the most important issue, because a very small amount of ammonia (ppm level) poisons the catalysts of proton exchange membrane (PEM) fuel cells. In this regard, sodium alanate has offered good prospects due to the high purity of its released hydrogen, its high reversible hydrogen storage capacity, and its optimal thermodynamic stability for reversible hydrogen storage at moderate temperatures, since Bogdanović and Schwickardi demonstrated that transition-metal dopants can considerably lower the kinetic barriers for both hydrogenation and dehydrogenation of $NaAlH_4$.[6] It is well known that $NaAlH_4$ decomposes to release hydrogen in three steps according to the following reactions:

$$NaAlH_4 \leftrightarrow 1/3Na_3AlH_6 + 2/3Al + 3/2H_2 \quad 3.7\ wt\%\ H_2 \quad (1)$$

$$Na_3AlH_6 \leftrightarrow 3NaH + Al + 3/2H_2 \quad 1.9\ wt\%\ H_2 \quad (2)$$

$$NaH \leftrightarrow Na + 1/2H_2 \quad 1.9\ wt\%\ H_2 \quad (3)$$

In principle, gives 3.7 wt% hydrogen and the second one 1.9 wt% upon heating. The last reaction, eqn (3), however, occurs at over 300 °C, releasing another 1.9 wt% of hydrogen. This temperature is high, and hence, the desorption of NaH is not considered a useful capacity for practical purposes. By doping with a few mol% of selected catalyst, $NaAlH_4$ can reversibly release and take up hydrogen, as described above for the first two-step reaction. During the past decade, various catalysts, such as carbon,[7] transition metal,[8] and rare earth metal[9] based materials have been found to be active in

[a]*Institute for Superconducting and Electronic Materials, University of Wollongong, NSW, 2522, Australia. E-mail: jeff.mao@hotmail.com; zguo@uow.edu.au*
[b]*School of Mechanical, Materials & Mechatronics Engineering, University of Wollongong, NSW, 2522, Australia*
† Electronic Supplementary Information (ESI) available. See DOI: 10.1039/c1ra00645b/

significantly enhancing the reaction kinetics of $NaAlH_4$. However, further improvements in the dehydriding and hydriding kinetics of $NaAlH_4$ are highly desirable. In addition, an understanding of the hydrogen desorption/absorption of $NaAlH_4$ doped with a metal based catalyst is still unclear. For example, several Ti-containing species including Ti–Al alloy, Ti hydrides, and Ti cations in the $NaAlH_4$ lattice are proposed as the active species in Ti doped $NaAlH_4$, but none of them has been conclusively confirmed.[8]

More recently, it was demonstrated that the catalytic effects of transition metals such as Ti and Zr combined with porous materials such as carbon nanotubes (CNTs) and porous SiO_2 as mixed dopants lead to significant acceleration of hydrogen dissociation and diffusion, approaching the goal of rapid hydrogenation kinetics at practically meaningful low temperatures.[10] For example, Wang *et al.*[10] found that all five carbons SWCNTs, multiwalled CNTs (MWCNTs), activated carbon (AC), fullerenes (C60), and graphite G) exhibited significant, sustaining, and synergistic co-catalytic effects on the dehydrogenation and hydrogenation kinetics of Ti-doped $NaAlH_4$ that persisted through charge and discharge cycling, in which SWCNTs were the best co-catalyst. This indicates that the synergistic interaction among metals and carbon nanotubes may be an effective strategy to significantly lower the operating temperature and to increase hydrogenation kinetics. Despite this progress, the dehydrogenation and hydrogenation kinetics still fall short of the requirements for practical applications. It is therefore desirable to further explore and develop the synergistic effects of CNTs with other metallic catalysts in order to achieve faster kinetics.

In our previous work, we demonstrated that the hydrogen desorption/absorption of $NaAlH_4$ can be significantly improved by introducing NbF_5 through the *in situ* formation of active Nb-containing catalysts and the function of F^- anions.[11] In this paper, we investigate the effects of single walled carbon nanotubes (SWCNTs) as a co-dopant on the hydrogen desorption/absorption of NbF_5-doped $NaAlH_4$. By comparing the hydrogen release/uptake kinetics with those of pristine $NaAlH_4$, SWCNT-doped $NaAlH_4$, and NbF_5-doped $NaAlH_4$, which possesses state-of-art kinetics among the various forms of doped $NaAlH_4$, we will show how SWCNTs can improve the hydrogen release/uptake kinetics of NbF_5-doped $NaAlH_4$ by a series of dehydrogenation/rehydrogenation measurements. Moreover, in order to acquire detailed information about the kinetics of the reactions, the non-isothermal Kissinger method has been used to evaluate the activation energy. At the end of the article, on the basis of these findings and the previous investigations, the active species and the catalysis are discussed.

Experimental procedures

The chemicals $NaAlH_4$ (hydrogen-storage grade, $\geqslant$93% purity), NbF_5 (98%), and single walled carbon nanotubes (SWCNTs) were all purchased from Sigma-Aldrich and used directly without pretreatment. All sample storage and handling were performed in an Ar filled glove box (MBraun Unilab). A QM-3SP2 planetary ball mill was employed to prepare the pristine $NaAlH_4$, $NaAlH_4$-3 mol% NbF_5, $NaAlH_4$-5 wt% SWCNT and $NaAlH_4$-3 mol% NbF_5-5 wt% SWCNT samples, under an argon atmosphere at 450 rpm. Each time, about 1 g of a sample was prepared with 2 h of ball milling, with a ball-to-powder ratio of around 30 : 1.

The hydrogen desorption/absorption properties were measured in a Sieverts apparatus (Advanced Materials Corporation, USA), where the temperatures and pressures of the sample and the gas reservoirs were monitored and recorded by GrcLV-LabVIEW-based control program software during the sorption process. Temperature programmed desorption (TPD) curves were determined by volumetric methods starting from vacuum. The temperature was increased from ambient to $\sim$300 °C at 2 °C min^{-1}. The hydrogen desorption kinetic measurements were performed at the desired temperature starting from vacuum. The hydrogen absorption measurements were performed at 150 or 160 °C and 55 or 65 bar hydrogen pressure. The sample was thoroughly dehydrogenated at 300 °C under dynamic vacuum before the rehydrogenation measurement. Other than specified, the H-capacity was calculated using the total weight of the samples to allow for an evaluation of the practical hydrogen storage properties.

Differential scanning calorimetry (DSC) analysis of the dehydrogenation process was carried out on a Mettler ToledoTGA/DSC 1. About 2–6 mg of the sample was loaded into an alumina crucible in the glove box. The crucible was then placed in a sealed glass bottle in order to prevent oxidation during transportation from the glove box to the DSC apparatus. An empty alumina crucible was used as the reference material. The samples were heated from room temperature to 300 °C under 1 atm flowing argon atmosphere, and the heating rate was 2 °C min^{-1}.

The phase structures of various samples at different stages were identified by a GBC X-ray diffractometer with Cu-Kα radiation at 40 kV and 25 mA. In order to avoid oxidation during the X-ray diffraction (XRD) measurement, samples were mounted on a glass slide 1 mm in thickness in the Ar-filled glove box and sealed with an airtight hood composed of amorphous tape. To obtain the information of Al–H bond, the obtained samples were ground with KBr and pressed into a sample cup, and the vibration spectra of the species were then identified using a Shimadzu Prestige 21 Fourier transform infrared spectrometer (FTIR) in absorbance mode.

Results and discussion

Hydrogen desorption

Fig. 1 reveals the effects of NbF_5 and the SWCNTs, when used separately as single catalysts or together as co-catalysts, on the dehydrogenation of $NaAlH_4$ by means of TPD curves. It was observed that the pristine $NaAlH_4$ starts to release a small amount of hydrogen at around 183 °C, which is probably due to the melting of $NaAlH_4$. Most of the hydrogen was released starting at 210 °C, and release was completed at 283 °C. The total amount of hydrogen evolved is about 5.5 wt%, which is very close to the theoretical value from eqn.(1) and (2), but these two steps of dehydrogenation were not distinct. In contrast, a significant catalytic effect was observed in the curves for the NbF_5-doped, SWCNT-doped, and NbF_5 and SWCNT co-doped samples, which exhibited two distinct dehydrogenation steps at much lower dehydrogenation temperatures. For the NbF_5-doped

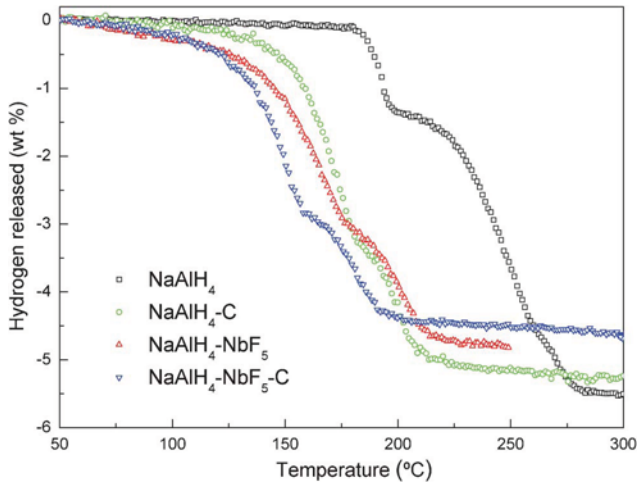

Fig. 1 Temperature programmed desorption (TPD) curves of as-milled $NaAlH_4$, and $NaAlH_4$ doped with different catalysts. The heating rate was 2 °C min^{-1}.

$NaAlH_4$ sample, the first-step dehydrogenation could be finished at around 178 °C. Further heating led to a second decomposition, which was completed at 225 °C. For the SWCNT-doped $NaAlH_4$ sample, the first and second dehydrogenation steps could be finished at 181 and 223 °C, respectively. Clearly, the dehydrogenation temperature of the $NaAlH_4$ is reduced by addition of either NbF_5 or SWCNTs, suggesting that a catalytic effect occurred. Furthermore, the NbF_5 and SWCNT co-doped $NaAlH_4$ sample can complete its first and second-step dehydrogenation at 159 and 201 °C, respectively, which is lower than for the NbF_5 or SWCNT-doped $NaAlH_4$ samples. These results clearly show the synergistic effects associated with the use of SWCNTs as a co-catalyst with NbF_5.

The aforementioned TPD results are confirmed by the DSC curves shown in Fig. 2. Clearly, the plot for the pristine $NaAlH_4$ shows four distinct endothermic processes, which can be assigned to the melting of $NaAlH_4$ (~185 °C), along with slight decomposition of the $NaAlH_4$, the decomposition of molten $NaAlH_4$ to Na_3AlH_6 (195–252 °C), a phase transition of α–Na_3AlH_6 to β–Na_3AlH_6 (~264 °C) and the decomposition of Na_3AlH_6 into NaH and Al (171–286 °C). However, only two endothermic peaks are seen in the dehydrogenation of the doped $NaAlH_4$ samples. In the case of the NbF_5-doped sample, the first peak at about 178 °C is attributed to the dehydrogenation of $NaAlH_4$, and the second peak at 215 °C corresponds to the dehydrogenation of Na_3AlH_6. For the SWCNT-doped sample, the first and second peaks were observed at 179 and 219 °C, corresponding to the decomposition of $NaAlH_4$ and Na_3AlH_6, respectively. As a whole, the DSC curves for the co-doped $NaAlH_4$ sample were similar to those of the NbF_5 or SWCNT doped samples, displaying only two endothermic peaks, corresponding to eqn. (1) and (2), respectively, but both endothermic peaks had moved to lower temperatures. The first peak at about 169 °C is attributed to the dehydrogenation of $NaAlH_4$, and the second peak at 209 °C corresponds to the dehydrogenation of Na_3AlH_6, which is lower than for either the NbF_5 or the SWCNT doped samples. These results further confirmed the synergistic effect of NbF_5 and SWCNTs towards the decomposition of $NaAlH_4$.

A comparative evaluation of the isothermal dehydrogenation kinetics of $NaAlH_4$ with single catalysts (NbF_5, SWCNTs) and co-catalysts (NbF_5 and SWCNTs together) at 155 °C was performed, as shown in Fig. 3. For the pristine $NaAlH_4$, no appreciable hydrogen desorption is detected within 120 min at 155 °C (results not shown here). However, the NbF_5-doped sample releases around 2.5 wt% hydrogen within 50 min. The hydrogen evolved from the SWCNT-doped $NaAlH_4$ sample is 2.4 wt% in 50 min, which is a little lower than for the NbF_5-doped sample. The results indicate that the hydrogen released from the SWCNT- and NbF_5-doped samples at 155 °C is attributable to the first-step dehydrogenation of $NaAlH_4$ according to eqn. (1). However, the dehydrogenation curves for the co-doped sample showed a two-step decomposition feature, corresponding to the first reaction stage (1) and the second reaction stage (2) of $NaAlH_4$, respectively. The co-doped sample releases about 2.5 wt% hydrogen in 6 min and another

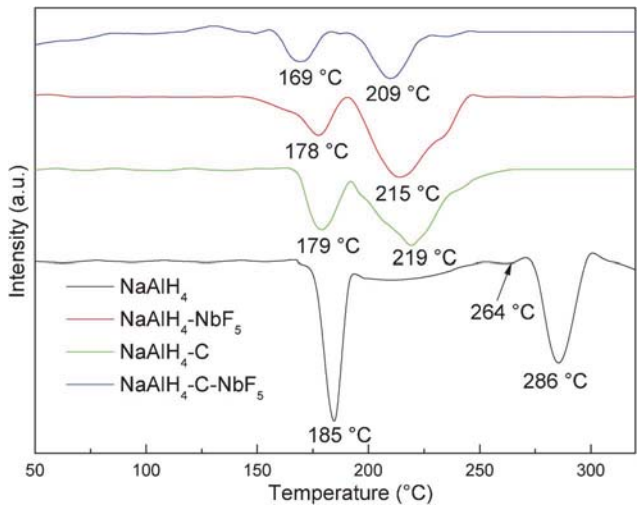

Fig. 2 Differential scanning calorimetry (DSC) curves of the $NaAlH_4$, $NaAlH_4$-3 mol% NbF_5, $NaAlH_4$-5 wt% SWCNT, and $NaAlH_4$-3 mol% NbF_5-5 wt% SWCNT samples.

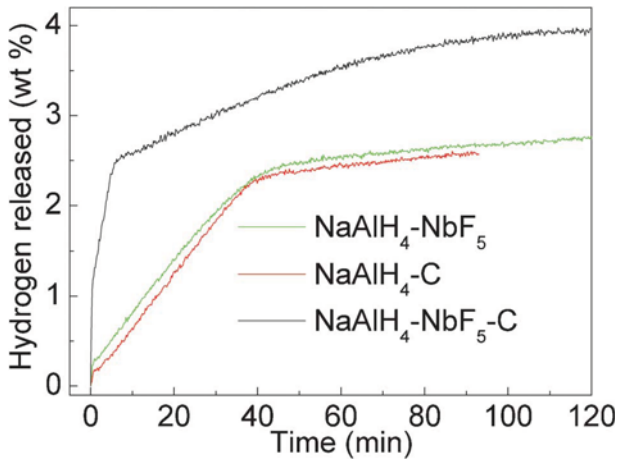

Fig. 3 Isothermal dehydrogenation curves at 155 °C for $NaAlH_4$-3 mol% NbF_5, $NaAlH_4$-5 wt% SWCNT, and $NaAlH_4$-3 mol% NbF_5-5 wt% SWCNT samples.

1.45 wt% in the following 120 min, almost all of the hydrogen in the post-milled sample. This phenomenon further indicates that a synergistic catalysis from the combination of NbF_5 and SWCNTs exists for $NaAlH_4$.

Hydrogen absorption

Fig. 4 presents a systematic comparison of the absorption behaviour between the $NaAlH_4$ samples with NbF_5 or SWCNTs as the sole additive and with NbF_5 and SWCNTs as co-additives. It was observed that the simultaneous addition of NbF_5 and SWCNTs further improves the absorption rate of $NaAlH_4$. At 150 °C and 55 bar in Fig. 4(a), the saturated hydrogenation process for the co-doped sample can be limited to within 20 min, which is lower than for the SWCNT doped sample (48 min) and much lower than for the NbF_5 doped sample (96 min). On increasing the hydrogenation temperature and pressure up to 160 °C and 6.5 MPa (see Fig. 4(b)), the rehydrogenation capacity remains unchanged for the three samples, but the absorption rate is increased, leading to saturated rehydrogenation times of 7, 14, and 49 min, respectively, for the co-doped, SWCNT doped, and NbF_5 doped samples. These results clearly show that the co-doped $NaAlH_4$ has better rehydrogenation kinetics than the samples doped with a single catalyst.

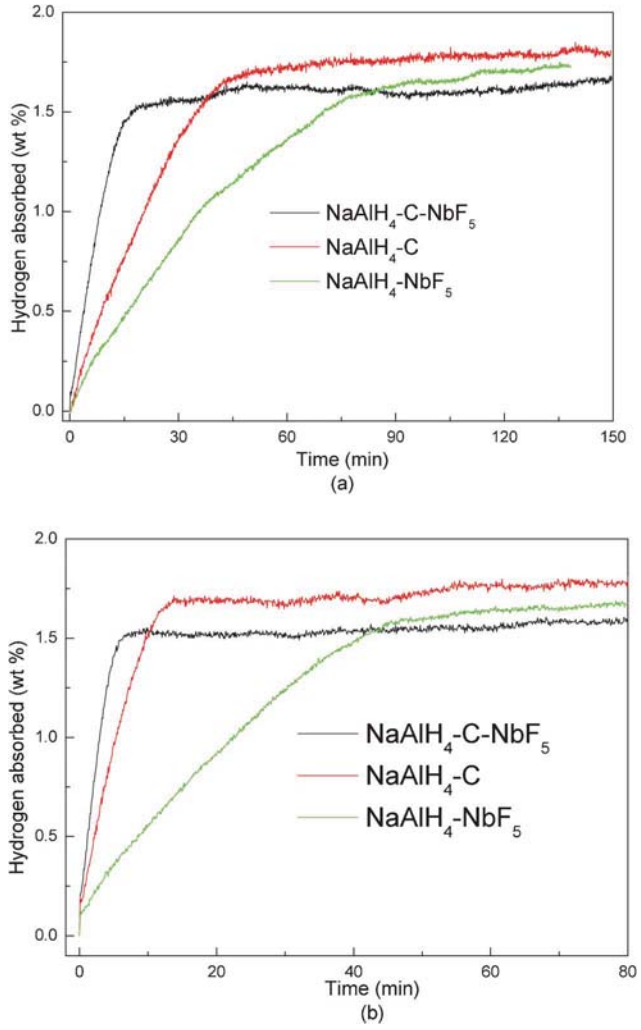

Fig. 4 Comparison of the hydrogenation curves for the first dehydrogenation cycle of $NaAlH_4$-3 mol% NbF_5, $NaAlH_4$-5 wt% SWCNT, and $NaAlH_4$-3 mol% NbF_5-5 wt% SWCNT samples at (a) 150 °C and 5.5 MPa H_2 pressure and (b) 160 °C and 6.5 MPa H_2 pressure.

It is worth noting that the rehydrogenation capacity for the SWCNT-doped, NbF_5-doped, and SWCNT–NbF_5 co-doped samples is 1.78, 1.73, and 1.66 wt%, respectively. These values are similar to those found in the second-step dehydrogenation processes in these three samples, suggesting that the hydrogen released from the rehydrogenated sample is from the separate contributions of the reformed Na_3AlH_6. To confirm this, these rehydrogenation products for the three samples were examined by means of TPD, and the TPD curves are compared in Fig. 5. Fig. 5 presents the TPD curves for the first hydrogenation cycle of the three samples. All the curves show one hydrogen release step, starting at over 150 °C and completed before 240 °C, with a hydrogen capacity of between 1.5–1.7 wt%. All in all, these results indicate the recombination of Na_3AlH_6 in all three samples. The absence of $NaAlH_4$ in the rehydrogenated state is possibly due to the quite high equilibrium hydrogen pressure required for the transformation from Na_3AlH_6 to $NaAlH_4$ in the hydrogenation process by eqn. (1).[12] Meanwhile, the dehydrogenation temperature for the rehydrogenated SWCNT doped sample is similar to that of the rehydrogenated NbF_5 doped sample. However, the co-doped sample has the lowest dehydrogenation temperature compared to the SWCNT and NbF_5 doped samples, further confirming the synergistic effect of NbF_5 and SWCNTs.

Structure analysis

An intriguing aspect of the co-doped $NaAlH_4$ sample after cycling through synthesis, dehydrogenation, and rehydrogenation is illustrated by the XRD patterns shown in Fig. 6. After ball milling, only peaks due to the $NaAlH_4$ and a small amount of Al are observed. The crystalline Al is most likely formed by the decomposition of a minor part of the $NaAlH_4$ during the ball milling, due to the effects of the NbF_5 and SWCNTs. Upon desorption of the hydrogen from the as-milled sample, the $NaAlH_4$ phase has disappeared, and more the crystalline Al and

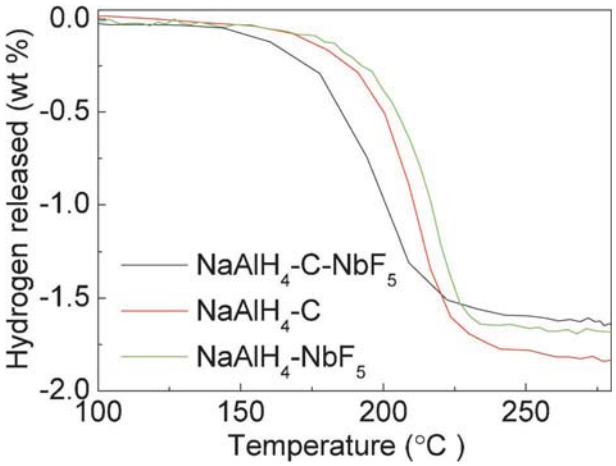

Fig. 5 TPD curves of the $NaAlH_4$-3 mol% NbF_5, $NaAlH_4$-5 wt% SWCNT, and $NaAlH_4$-3 mol% NbF_5-5 wt% SWCNT samples for the first rehydrogenation.

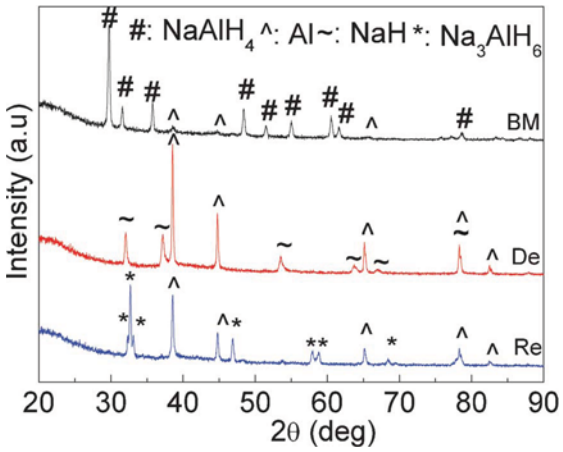

Fig. 6 XRD patterns of the $NaAlH_4$-3 mol% NbF_5-5 wt% SWCNT samples after ball milling (BM), of the milled sample after dehydrogenation (De), and of the dehydrogenated sample after rehydrogenation (Re).

NaH are observed, indicating the complete decomposition of $NaAlH_4$ according to eqn. (1) and eqn. (2). After rehydrogenation, the peak due to the crystalline Al decreases in height, and the new phase Na_3AlH_6 is formed. Nevertheless, no crystalline $NaAlH_4$ is formed, which is possibly due to the quite high equilibrium hydrogen pressure required for the transformation of Na_3AlH_6 to $NaAlH_4$ in the hydrogenation process by eqn. (1). However, no C, Nb-, or F-containing species could be detected in the co-doped sample in the different stages, which may be attributed to the low concentration (NbF_5) or amorphous state (C) in the sample.

In order to detect the existing state of C, Nb and F in the NbF_5 and SWCNT co-doped $NaAlH_4$ sample, two samples of $NaAlH_4$-30 wt% NbF_5-15 wt% SWCNT and $NaAlH_4$-60 wt% NbF_5-30 wt% SWCNT were further prepared by increasing the amount of NbF_5 and SWCNT. Then, the XRD patterns of the as-milled samples were analysed, as shown in Fig. 7. Clearly, only $NaAlH_4$ and Al phases were observed in the case of $NaAlH_4$-30 wt% NbF_5-15 wt% SWCNT. However, for the $NaAlH_4$-60 wt% NbF_5-30 wt% SWCNT samples, the $NaAlH_4$ phase disappeared. Meanwhile, in addition to Al, the new phases of Al_3Nb, $NbHx$, and NaF were identified although their diffraction peaks are weak and distorted (Fig. 7 and Fig. S1, ESI†). Since $NaAlH_4$ was stable when it was ball milled alone,[11] the consumption of $NaAlH_4$ and the formation of Al_3Nb, $NbHx$, and NaF in the case of $NaAlH_4$-60 wt% NbF_5-30 wt% SWCNT were very likely due to a chemical reaction between $NaAlH_4$ and NbF_5. The result agrees well with our previous report that Al_3Nb, $NbHx$, and NaF were also detected in the NbF_5 doped $NaAlH_4$ sample after ball milling.[11] Therefore, it can be deduced that similar to the case of NbF_5 doped $NaAlH_4$, the NbF_5 still prefer to react with $NaAlH_4$ during ball milling to generate the active Nb and F containing species in the case of NbF_5 and SWCNT co-doped sample.

The FTIR spectra for the pure, NbF_5 doped, SWCNT doped, and co-doped $NaAlH_4$ are compared in Fig. 8, in which two intense bands appear at 1694 cm^{-1} and 866 cm^{-1}, which are attributed to the v_3 $[AlH_4]^-$ stretching and v_4 $[AlH_4]^-$ bending modes, respectively. In comparison with the pristine sample, the host bands for the doped samples remain unchanged in position, but are reduced in intensity. The observed reduction in the stretching and bending bands is indicative of the weakening of the Al–H bonds in the $NaAlH_4$ lattice, which cause hydrogen to desorb at lower temperatures, as well as facilitating the absorption of H_2 to reverse the dehydrogenation reaction. Moreover, the co-doped sample displayed the weakest intensity, indicating that a synergetic effect between NbF_5 and SWCNTs may be present.

Activation energy

To further study the effect of the co-catalyst on the kinetic barrier, the apparent activation energy (E_a) relating to the first and the second-step dehydrogenation of $NaAlH_4$ was estimated using the non-isothermal Kissinger method according to the following equation.[13]

$$\ln(\beta/T_m^2) = -E_a/RT \quad (4)$$

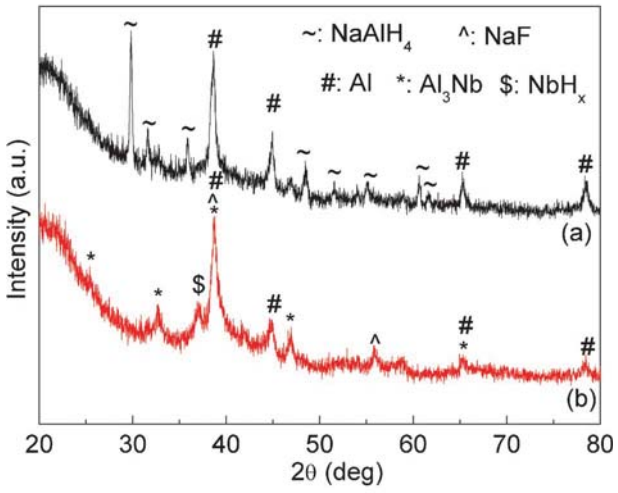

Fig. 7 XRD patterns of the (a) $NaAlH_4$-30 wt% NbF_5-15 wt% SWCNT and (b) $NaAlH_4$-60 wt% NbF_5-30 wt% SWCNT samples after ball milling.

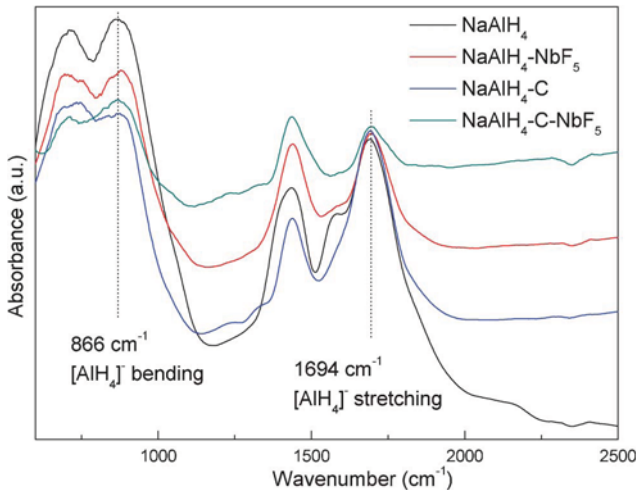

Fig. 8 FTIR spectra of $NaAlH_4$, $NaAlH_4$-3 mol% NbF_5, $NaAlH_4$-5 wt% SWCNT, and $NaAlH_4$-3 mol% NbF_5-5 wt% SWCNT samples after ball milling.

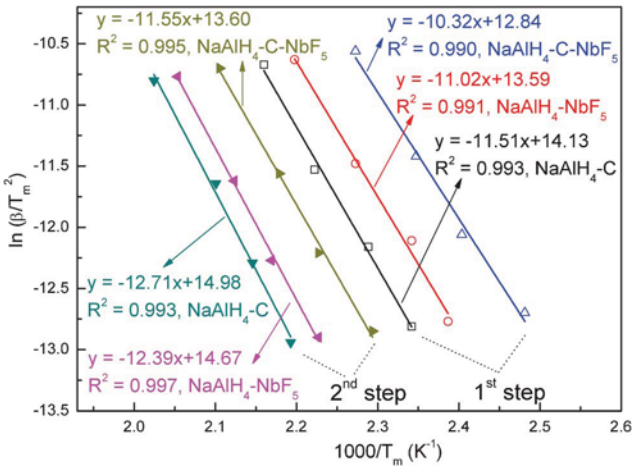

Fig. 9 Kissinger plots for the first and second dehydrogenation steps for the $NaAlH_4$-3 mol% NbF_5, $NaAlH_4$-5 wt% SWCNT, and $NaAlH_4$-3 mol% NbF_5-5 wt% SWCNT samples.

Where E_a is the activation energy, β is the heating rate in °C min^{-1}, T_m is the absolute temperature for the maximum desorption rate, and R is the gas constant. In this work, T_m was obtained using TPD measurement with the selected heating rates of 0.5, 1, 2 and 5 °C min^{-1}. The detailed TPD curves are shown in Figures S2–S4 of the ESI.† Plotting $\ln(\beta/T_m^2)$ *versus* $1/T_m$ yields a straight line with the slope of $-E_a/R$. Fig. 9 shows the Kissinger plots for the first-step and second-step dehydrogenation of the co-doped $NaAlH_4$ sample, together with NbF_5– and SWCNT-doped samples for comparison. The intrinsic linearity of all of the curves indicates that the dehydrogenation kinetics of doped $NaAlH_4$ is well represented by the non-isothermal Kissinger equation and that they follow a first order decomposition reaction.

The derived values of the activation energies, E_{a1}, for the first step [*i.e.*, eqn. (1)] and E_{a2} for the second step [*i.e.*, eqn. (2)], are listed in Table 1. For comparison, E_{a1} and E_{a2} of pristine $NaAlH_4$ are also included in Table 1.[14] Comparison of the activation energies for dehydrogenation reveals several phenomena as follows: (1) All of the present additives significantly enhance the dehydrogenation kinetics of $NaAlH_4$ and Na_3AlH_6 (reducing E_{a1} and E_{a2}). (2) SWCNTs enhance the kinetics of $NaAlH_4$, reducing E_{a1} from 118.1 to 95.8 kJ mol^{-1}, and E_{a2} from 120.7 to 105.8 kJ mol^{-1}, showing that the addition of SWCNTs reduces energy barriers for both eqn.(1) and eqn. (2). (3) Compared to the SWCNT doped sample, the NbF_5 doped sample has a lower E_{a1} (91.7 kJ mol^{-1}) and E_{a2} (103.1 kJ mol^{-1}), indicating that NbF_5 is more effective for the decomposition of $NaAlH_4$. It should be noted that the activation energies for the decomposition of NbF_5 doped $NaAlH_4$ are slightly different to that of our previous report, which is probably due to the fact that the T_m was obtained using TPD measurement in this paper but using DSC measurement in the previous report.[11] (3) The combination of SWCNTs and NbF_5 was more efficient than those of SWCNTs or NbF_5 alone, lowering the E_{a1} and E_{a2} to 85.9 and 96.2 kJ mol^{-1}, respectively. This phenomenon indicates that a synergistic catalytic effect between the NbF_5 and SWCNTs exists for $NaAlH_4$.

Table 1 Apparent Activation Energies (E_a) for the first-step and second-step dehydrogenation of $NaAlH_4$, respectively

Samples	E_{a1} (kJ mol^{-1})	E_{a2} (kJ mol^{-1})
$NaAlH_4$	118.1	120.7
$NaAlH_4$–NbF_5	91.7	103.1
$NaAlH_4$–C	95.8	105.8
$NaAlH_4$–C–NbF_5	85.9	96.2

Discussion

On the basis of the above results, it is evident that the dehydrogenation and rehydrogenation kinetics of $NaAlH_4$ were enhanced by introducing NbF_5 or SWCNTs. As discussed in our previous paper,[11] a much higher dispersion of Nb–Al and Nb–H active species may form on the hydride surface or grain boundaries during ball milling or after the heating process in the NbF_5–doped $NaAlH_4$, which may facilitate the dissociation/recombination of molecular hydrogen and mass transport. Meanwhile, the introduction of F-anions may also play a role, which has also been theoretically and experimentally demonstrated in the study of $NaAlH_4$.[15] Therefore, it was believed that both Nb and F containing species play critical roles in the dehydrogenation/hydrogenation process of the $NaAlH_4$ sample with added NbF_5. The reasons for the improvement in the dehydrogenation of $NaAlH_4$ doping with SWCNTs can be understood from the following three aspects: (1) SWCNTs exhibits a prominent "catalytic" effect in $NaAlH_4$. Based on the experimental observations and theoretical calculations, Berseth *et al.* provided a general understanding of the catalytic mechanism by the carbon catalysts that interaction of $NaAlH_4$ with an electronegative substance such as carbon nanotube affects the charge donation from Na to AlH_4, consequently weakening the Al–H bond and decreasing the dehydrogenation temperatures as well as facilitating the rehydrogenation reaction.[7] Actually, the weakening of Al–H bond in the $NaAlH_4$ lattice was confirmed by FTIR in the case of $NaAlH_4$-5 wt% SWCNTs, compared with pristine $NaAlH_4$ sample (Fig. 8). (2) Because of the nanosize and strength, the SWCNTs can penetrate in $NaAlH_4$ matrix either nearly vertically or in an inclined orientation. Therefore, the presence of SWCNTs may facilitate the atomic hydrogen diffusion both inside the phase grains and along the grain boundaries. (3) The presence of SWCNTs may also modify the grain interfaces of dehydrogenated phases due to its high specific surface area, especially by inhibiting the aggregation of Al particles. All these are responsible for the decrease in both the onset dehydrogenation temperature and the activation energy in the SWCNT-doped $NaAlH_4$.

It was also shown that co-doping with NbF_5 and SWCNTs exhibits superior de/rehydrogenation properties to that doping with single NbF_5 or SWCNTs, indicating a favorable synergistic effect. It is already well known that combined utilization of catalytically active metal nanoparticles and nanostructured carbon materials is effective for improving the dehydriding/rehydriding properties of metal hydrides, and this strategy has been intensely developed over the past several decades,[10,16] where the carbon nanotubes are expected to form a net-like structure after being milled together with host metal hydrides,

thus creating a microconfined environment for the decomposition/restoration of hydrides, while the metal nanoparticles have high catalytic activity. In our case, we also believe that both NbF_5 and SWCNTs play important roles in the dehydrogenation/hydrogenation process of the co-doped $NaAlH_4$. Similar to the NbF_5 doped $NaAlH_4$, the active species of $NbHx$, Al_3Nb, and NaF were also found in the co-doped sample (Fig. 7).[11] The results indicate that NbF_5 prefers to react with $NaAlH_4$ during ball milling to generate the active Nb and F containing species in the NbF_5 and SWCNT co-doped sample. The role of SWCNTs in the co-doped sample could be more ''physical'' than ''chemical'' compared with the catalytic role of NbF_5 in that it modifies the grain surface of the dehydrogenated phases probably due to the inhibition of grain aggregation. As a consequence, a favourable synergistic effect on the dehydrogenation and rehydrogenation of $NaAlH_4$ is achieved in the co-doped $NaAlH_4$ sample through the formation of Nb- and F- containing species, and the presence of SWCNTs. All these complex factors resulted in together the improvement of the hydrogen storage performances of $NaAlH_4$.

Conclusions

The effects of SWCNTs as a co-catalyst with NbF_5 on the dehydrogenation and hydrogenation kinetics of $NaAlH_4$ are presented in the present study. Either the SWCNTs or the NbF_5 alone can improve the hydrogen de/absorption properties of $NaAlH_4$. Moreover, a synergistic effect on the dehydrogenation of $NaAlH_4$ occurs when SWCNTs are added as a co-dopant with NbF_5. For example, the synergistic effect results in the apparent activation energy for the first-step and the second-step dehydrogenation of $NaAlH_4$ being reduced to 85.9 kJ mol^{-1} and 96.2 kJ mol^{-1}, respectively. These positive effects can be ascribed to the *in situ* formation of Nb- and F- containing species in the NbF_5, as well as the presence of nanosized pores and the high specific surface area of the SWCNTs.

Acknowledgements

We would like to acknowledge support from the University of Wollongong, as well as critical reading by Dr Tania Silver.

References

1 (*a*) V. Mehta and J. S. Cooper, *J. Power Sources*, 2003, **114**, 32; (*b*) V. M. Vishnyakov, *Vacuum*, 2006, **80**, 1053.
2 (*a*) L. Schlapbach and A. Zuttel, *Nature*, 2001, **414**, 353; (*b*) S. V. Alapati, J. Karl Johnson and D. S. Sholl, *Phys. Chem. Chem. Phys.*, 2007, **9**, 1438.
3 (*a*) A. Züttel, S. Rentsch, P. Fischer, P. Wenger, P. Sudan, P. Mauron and C. Emmenegger, *J. Alloys Compd.*, 2003, **356-357**, 515; (*b*) S. Orimo, Y. Nakamori, G. Kitahara, K. Miwa, N. Ohba, S. Towata and A. Züttel., *J. Alloys Compd.*, 2007, **404**, 427; (*c*) P. Mauron, F. Buchter, O. Friedrichs, A. Remhof, M. Bielmann, N. Z. Christoph and A. Züttel, *J. Phys. Chem. B*, 2008, **112**, 906; (*d*) P. Martelli, R. Caputo, A. Remhof, P. Mauron, A. Borgschulte and A. Züttel., *J. Phys. Chem. C*, 2010, **114**, 7173; (*e*) J. F. Mao, Z. P. Guo, X. B. Yu and H. K. Liu, *J. Phys. Chem. C*, 2011, **115**, 9283; (*f*) E. Rönnebro and E. Majzoub, *J. Phys. Chem. B*, 2007, **111**, 12045; (*g*) Y. Y.Kim, D. Reed, Y. S. Lee, J. Y. Lee, J. H. Shim, D. Book and Y. W. Cho, *J. Phys. Chem. C*, 2009, **113**, 5865; (*h*) J. F. Mao, Z. P. Guo, C. K. Poh, A. Ranjbar, Y. H. Guo, X. B. Yu and H. K. Liu, *J. Alloys Compd.*, 2010, **500**, 200; (*i*) K. Chzopek, C. Frommen, A. Leon, O. Zabara and M. Fichtner, *J. Mater. Chem.*, 2007, **17**, 3496; (*j*) H. W. Li, K. Kikuchi, Y. Nakamori, N. Ohba, K. Miwa, S. Towata and S. Orimo, *Acta Mater.*, 2008, **56**, 1342; (*k*) G. Severa, E. Rönnebro and C. M. Jensen, *Chem. Commun.*, 2010, **46**, 421.
4 (*a*) P. Chen, Z. T. Xiong, J. Luo, J. Lin and K. Tan, *Nature*, 2002, **420**, 302; (*b*) W. F. Luo, *J. Alloys Compd.*, 2004, **381**, 284; (*c*) H. Y. Leng, T. Ichikawa, S. Hino, N. Hanada, S. Isobe and H. Fujii, *J. Phys. Chem. B*, 2004, **108**, 8763; (*d*) Y. F. Liu, K. Zhong, M. X. Gao, J. H. Wang, H. G. Pan and Q. D. Wang, *Chem. Mater.*, 2008, **20**, 3521; (*e*) Z. T. Xiong, C. K. Yong, G. Wu, P. Chen, W. Shaw, A. Karkamkar, T. Autrey, M. O. Jones, S. R. Johnson, P. P. Edwards and W. I. F. David, *Nat. Mater.*, 2008, **7**, 138.
5 (*a*) J. Chen, N. Kuriyama, Q. Xu, H. T. Takeshita and T. Sakai, *J. Phys. Chem. B*, 2001, **105**, 11214; (*b*) J. R. Ares, K. F. Aguey-Zinsou, F. Leardini, I. J. Ferrer, J. F. Fernandez, Z. X. Guo and C. Sánchez., *J. Phys. Chem. C*, 2009, **113**, 6845; (*c*) Y. Y. Kim, E. K. Lee, J. H. Shim, Y. W. Cho and K. B. Yoon, *J. Alloys Compd.*, 2006, **422**, 283; (*d*) N. Hanada, W. Lohstroh and M. Fichtner, *J. Phys. Chem. C*, 2008, **112**, 131; (*e*) F. H. Wang, Y. F. Liu, M. X. Gao, K. Luo, H. P. Pan and Q. D. Wang, *J. Phys. Chem. C*, 2009, **113**, 7978.
6 B. Bogdanović and M. Schwickardi, *J. Alloys Compd.*, 1997, **253-#x2013;254**, 1.
7 (*a*) J. Wang, A. D. Ebner, T. Prozorov, R. Zidan and J. A. Ritter, *J. Alloys Compd.*, 2005, **395**, 252; (*b*) A. Zaluska, L. Zaluski and J. O.Ström-Olsen, *J. Alloys Compd.*, 2000, **298**, 125; (*c*) P. Adelhelm, K. P. de Jong and P. E. de Jongh., *Chem. Commun.*, 2009, **41**, 6261; (*d*) P. A. Berseth, A. G. Harter, R. Zidan, A. Blomqvist, C. M. Araujo, R. H. Scheicher, R. Ahuja and P. Jena, *Nano Lett.*, 2009, **9**, 1501; (*e*) C. Cento, P. Gislon, M. Bilgili, A. Masci, Q. Zheng and P. P. Prosini, *J. Alloys Compd.*, 2007, **437**, 360; (*f*) M. Hudson, H. Raghubanshi, D. Pukazhselvan and O. Srivastava, *Int. J. Hydrogen Energy*, 2011, DOI: 10.1016/j.ijhydene.2011.03.003; (*g*) A. C. Stowea, J. A. Teprovich, D. A. Knighta, M. S. Wellonsa and R. Zidan, *J South Carolina Academy of Science*, 2011, **9**, 13.
8 (*a*) K. J. Gross, E. H. Majzoub and S. W. Spangler, *J. Alloys Compd.*, 2003, **356–357**, 423; (*b*) D. L. Sun, S. Srinivasan, T. Kiyobayashi, N. Kuriyama and C. Jensen, *J. Phys. Chem. B*, 2003, **107**, 10176; (*c*) P. Wang and C. M. Jensen, *J. Alloys Compd.*, 2004, **379**, 99; (*d*) S. Gomes, G. Renaudin, H. Hagemann, K. Yvon, M. P. Sulic and C. M. Jensen, *J. Alloys Compd.*, 2005, **390**, 305; (*e*) H. Brinks, M. Sulic, C. M. Jensen and B. Hauback, *J. Phys. Chem. B*, 2006, **110**, 2740; (*f*) F. Fang, J. Zhang, J. Zhu, G. R. Chen, D. L. Sun, B. He, Z. Wei and S. Q. Wei, *J. Phys. Chem. C*, 2007, **111**, 3476; (*g*) X. D Kang, P. Wang and H. M. Cheng, *Int. J. Hydrogen Energy*, 2007, **32**, 2943; (*h*) A. Léon, G. Yalovega, A. Soldatov and M. Fichtner, *J. Phys. Chem. C*, 2008, **112**, 12545; (*i*) X. Z. Xiao, L. X. Chen, X. L. Fan, X. Wang, C. Chen C, Y. Q. Lei and Q. D. Wang, *Appl. Phys. Lett.*, 2009, **94**, 041907; (*j*) Y. F. Liu, C. Liang, H. Zhou, M. X. Gao, H. G. Pan and Q. D. Wang, *Chem. Commun.*, 2011, **47**, 1740; (*k*) H. Wang, A. Tezuka, H. Ogawa and T. Ikeshoji, *Phys. Rev. B: Condens. Matter Mater. Phys.*, 2011, **83**, 045112; (*l*) T. J. Frankcombe, G. J. Kroes, N. I. Choly and E. Kaxiras, *J. Phys. Chem. B*, 2005, **109**, 16554.
9 (*a*) B. Bogdanović, M. Felderhoff, A. Pommerina, F. Schüth, S. Nick and A. Starka, *J. Alloys Compd.*, 2009, **471**, 383; (*b*) C. Rongeat, N. Scheerbaum, L. Schultz and O. Gutfleisch, *Acta Mater.*, 2011, **59**, 1725; (*c*) X. L. Fan, X. Z. Xiao, L. X. Chen, K. R. Yu, Z. Wu, S. Q. Li and Q. D. Wang, *Chem. Commun.*, 2009, **44**, 6857; (*d*) Y. Suttisawat, V. Jannatisin, P. Rangsunvigit, B. Kitiyanan, N. Muangsin and S. Kulprathipanja, *Int. J. Hydrogen Energy*, 2007, **32**, 1277; (*e*) T. Sun, B. Zhou, H. Wang and M. Zhu, *Int. J. Hydrogen Energy*, 2008, **33**, 2260; (*f*) G. Lee, J. Shim, Y. Cho and K. Lee, *Int. J. Hydrogen Energy*, 2007, **32**, 1911; (*g*) D. Pukazhselvan, M. Sterlin Leo Hudson, B. K. Gupta, M. A. Shaz and O. N. Srivastava, *J. Alloys Compd.*, 2007, **439**, 243.
10 (*a*) J. Wang, A. D. Ebner and J. A. Ritter, *J. Phys. Chem. B*, 2006, **110**, 17353; (*b*) Z. Dehouche, L. Lafi, N. Grimard, J. Goyette and R. Chahine, *Nanotechnology*, 2005, **16**, 402; (*c*) S. Y. Zheng, Y. T. Li, F. Fang, G. Y. Zhou, X. B. Yu, G. R. Chen, D. L. Sun, L. Z. Ouyang and M. Zhu, *J. Mater. Res.*, 2010, **25**, 2047; (*d*) J. Ma, J. Li, R. Tang, D. W. Li, W. Z. Li an and Q. Y. Chen., *Int. J. Hydrogen Energy*, 2011, **36**, 9091; (*e*) Y. Suttisawat, P. Rangsunvigit, B. Kitiyanan and S. Kulprathipanja, *J. Solid State Electrochem.*, 2010, **14**, 1813.
11 J. F. Mao, Z. P. Guo and H. K. Liu, *Int. J. Hydrogen Energy*, 2011, **36**, 14503–14511.

12 (*a*) C. M. Jensen and K. J. Gross, *Appl. Phys. A: Mater. Sci. Process.*, 2001, **72**, 213; (*b*) B. Bogdanović, R. A. Brand, A. Marjanovic, M. Schwickardi and J. Tölle., *J. Alloys Compd.*, 2000, **302**, 36.
13 H. E. Kissinger, *Anal. Chem.*, 1957, **29**, 1702.
14 G. Sandrock, K. Gross and G. Thomas, *J. Alloys Compd.*, 2002, **399**, 299.
15 (*a*) L. C. Yin, P. Wang, X. D. Kang, C. H. Sun and H. M. Cheng, *Phys. Chem. Chem. Phys.*, 2007, **9**, 1499; (*b*) S. Singh and S. W. H. Eijt, *Phys. Rev. B: Condens. Matter Mater. Phys.*, 2008, **78**, 224110; (*c*) X. D. Kang, P. Wang and H. M. Cheng, *Scr. Mater.*, 2007, **56**, 361; (*d*) H. W. Brinks, A. Fossdal and B. C. Hauback, *J. Phys. Chem. C*, 2008, **112**, 5658; (*e*) Y. F. Liu, F. H. Wang, Y. H. Cao, M. X. Gao, H. G. Pan and Q. D. Wang, *Energy Environ. Sci.*, 2010, **3**, 645.
16 (*a*) X. D. Yao, C. Z. Wu, A. J. Du, J. Zou, Z. H. Zhu, P. Wang, H. M. Cheng, . S. Smith and G. Q. Lu, *J. Am. Chem. Soc.*, 2007, **129**, 15650; (*b*) Z. Z. Fang, X. D. Kang, P. Wang and H. M. Cheng, *J. Phys. Chem. C*, 2008, **112**, 17023.